Supplementary information for:

Riverine anaerobic ammonium oxidation across contrasting geologies

K. Lansdown,[1,2] B.A McKew,[3] C. Whitby,[3] C.M. Heppell[2], A.J. Dumbrell,[3] A. Binley,[4] L. Olde,[1] and M. Trimmer[1,*]

Affiliations:

1. School of Biological and Chemical Sciences, Queen Mary University of London, Mile End Road, London E1 4NS, United Kingdom.
2. School of Geography, Queen Mary University of London, Mile End Road, London E1 4NS, United Kingdom.
3. School of Biological Sciences, University of Essex, Wivenhoe Park, Colchester CO4 3SQ, United Kingdom.
4. Lancaster Environment Centre, Lancaster University, Lancaster, LA1 4YQ, United Kingdom

*Corresponding author: M. Trimmer, m.trimmer@qmul.ac.uk

CONTENTS Page Number

Supplementary Tables

Table S1: Location of sampling sites in the Hampshire Avon catchment

Site Label	River	Latitude	Longitude	*in situ* study
Clay 1	Sem	51.045826	-2.1104425	✓
Clay 2	Sem (tributary)	51.055413	-2.1568407	✓
Clay 3	Sem (tributary)	51.066347	-2.1431386	
Sand 1	Nadder	51.043849	-2.1118158	✓
Sand 2	Avon (west branch)	51.318289	-1.8600020	✓
Sand 3	Avon (west branch)	51.306169	-1.8227099	
Chalk 1	Ebble	51.027499	-1.9217089	✓
Chalk 2	Wylye	51.142475	-2.2033140	✓
Chalk 3	Avon (east branch)	51.304644	-1.8100633	

Table S2: Summary characteristics of un-vegetated sediments and river flow during sample collection and *in situ* activity measurements

	Grainsize (%)[†]				Organic C	N	C:N	Flow (m^3 s^{-1})[§]		Mixing	
Site	Clay	Silt	Sand	> 2 mm	(μmol g^{-1} dw)[‡]	(μmol g^{-1} dw)[‡]	(molar ratio)[‡]	Mean ± s.d.	Maximum	depth (cm)[#]	BFI[^]
Clay 1	6.3	16.0	65.5	12.0	1945 ± 499	114 ± 24	17 ± 1	0.04 ± 0.02	0.87	0	0.372
Clay 2	23.2	48.3	23.8	4.3	5499 ± 382	352 ± 19	16 ± 0.4	0.00 ± 0.00	1.17	0	0.234
Clay 3[*]					2465 ± 544	136 ± 23	17 ± 2				
Sand 1	0.5	1.3	80.7	17.4	492 ± 162	23 ± 6	23 ± 4	0.18 ± 0.02	2.28	1	0.695
Sand 2	1.7	2.9	90.9	4.4	351 ± 61	32 ± 4	11 ± 0.5	0.19 ± 0.09	2.76	8	0.861
Sand 3[*]					402 ± 66	38 ± 6	11 ± 1				
Chalk 1	0.4	1.1	45.5	52.8	692 ± 94	50 ± 11	15 ± 1	ND	3.77	6	0.953
Chalk 2	0.8	1.8	36.8	60.5	414 ± 50	39 ± 2	11 ± 1	0.09 ± 0.02	3.05	3	0.931
Chalk 3[*]					3530 ± 1470	234 ± 49	15 ± 3				

[*]Sites Clay 3, Sand 3 and Chalk 3 were only visited once to collect sediment for this current research and therefore, limited data are available. All other sites were part of a larger parent project that spanned April 2013 to November 2015. [†]Data are average values (n = 5). Particle size determination (<2 mm) was performed on a LS 13 320 Beckman Coulter Counter after treatment with 30 % hydrogen peroxide to remove organic matter. [‡]Organic C, N and C:N data are mean ± 1 standard error (n = 5). Sediment organic C and N content was determined by elemental analysis (Sercon Integra2) on material < 2mm after treatment with 1 M HCl to remove inorganic carbon. [§]Mean flow data are from the 2013 base-flow period (1/6 - 21/9/2013, n > 88). The flow gauge at site Chalk 1 was not operational during this time. Maximum flow data are peak flows recorded during the parent project (1/6/2013 - 13/5/2015). [#]Depth of groundwater - surface water mixing was determined by chloride depth profiles of porewaters recovered prior to the injection of ^{15}N, *see* ref. 1. ^BFI denotes base-flow index.

Table S3: *hzo* (hydrazine oxidoreductase) gene abundance (left) and relative abundance (right) in river sediments. Data are means ± 1 standard error.

Site Label	*hzo* gene abundance					
	hzo copies (g^{-1} d.w sediment)			*hzo* copies (10^6 16S rRNA copies)$^{-1}$		
Clay 1	6.78×10^5	±	2.51×10^5	52	±	12
Clay 2	3.90×10^5	±	1.86×10^5	90	±	44
Clay 3	2.79×10^5	±	4.63×10^4	72	±	7
Sand 1	5.27×10^5	±	3.65×10^4	308	±	22
Sand 2	9.23×10^5	±	2.08×10^5	569	±	286
Sand 3	2.44×10^6	±	7.95×10^4	978	±	863
Chalk 1	3.68×10^6	±	4.69×10^5	2768	±	572
Chalk 2	9.65×10^5	±	4.89×10^5	587	±	295
Chalk 3	3.34×10^6	±	8.13×10^4	2220	±	533

Table S4: Production of ^{15}N-N_2 as either $^{29}N_2$ or $^{30}N_2$ (P_{29} and P_{30}, respectively) in assays used to determine anammox potential in riverine sediments. Data are means (nmol N_2 g^{-1} h^{-1}) ± 1 standard error.

	$^{15}NH_4^+$		$^{15}NH_4^+$ and $^{14}NO_3^-$		$^{15}NO_3^-$	
Site Label	P_{29}	P_{30}	P_{29}	P_{30}	P_{29}	P_{30}
Clay 1	0.01 ± 0.01*	0.00 ± 0.01*	0.03 ± 0.01	-0.04 ± 0.02*	1.0 ± 0.1	18 ± 2
Clay 2	0.01 ± 0.00*	0.03 ± 0.03*	0.03 ± 0.02	0.01 ± 0.04*	4.8 ± 1.3	87 ± 19
Clay 3	0.01 ± 0.01*	0.01 ± 0.01*	0.09 ± 0.02	-0.01 ± 0.01*	1.9 ± 0.5	43 ± 9
Sand 1	0.01 ± 0.00*	0.01 ± 0.01*	1.1 ± 0.2	0.09 ± 0.05*	5.3 ± 1.2	29 ± 8
Sand 2	0.01 ± 0.01*	-0.01 ± 0.02*	1.1 ± 0.3	0.03 ± 0.02*	3.7 ± 0.4	41 ± 7
Sand 3	0.00 ± 0.00*	0.00 ± 0.01*	1.2 ± 0.2	0.02 ± 0.01*	11 ± 1	75 ± 10
Chalk 1	-0.01 ± 0.01*	0.01 ± 0.01*	1.4 ± 0.7	0.01 ± 0.01*	7.3 ± 2.0	61 ± 17
Chalk 2	-0.04 ± 0.02*	0.01 ± 0.03*	0.3 ± 0.2	-0.04 ± 0.04*	6.9 ± 0.7	66 ± 9
Chalk 3	-0.02 ± 0.01*	-0.02 ± 0.01*	2.5 ± 1.2	0.08 ± 0.06*	23 ± 9	218 ± 64

*Below detection limit. Classification of data as below the limit of detection was based upon increase of ratios of mass spectrometer signals for individual samples relative to a control. With the dimensions used in these slurries, this equates to approximately 0.03 and 0.4 nmol N_2 g^{-1} h^{-1} for P_{29} and P_{30}, respectively.

Table S5: Results from log likelihood tests on linear mixed effects models testing the effect of sediment type (catchment geology or permeability) on rates of anammox and contribution of anammox to N_2 production from both potential and *in situ* experiments.

Experiment	Dependent variable	Independent variable	df	χ^2	*p*-value
Potential	Total anammox	Geology (all)	2	8.05	0.018
		Sand, chalk	1	1.00	0.318
		Permeability	1	11.39	<0.001
Potential	Contribution (%)	Geology (all)	2	12.39	0.002
		Sand, chalk	1	1.27	0.260
		Permeability	1	11.51	<0.001
in situ	Ambient anammox	Geology (all)	2	4.55	0.103
		Permeability	1	0.06	0.812
in situ	Contribution (%)	Geology (all)	2	15.50	<0.001
		Sand, chalk	1	2.92	0.087
		Permeability	1	8.71	0.003

Table S6: BLASTn analysis of the 100 most abundant OTUs (representing between 92-93% of the total *hzo* gene sequences recovered).

OTUs	Closest relative (*hzo* clone name and Environmental source)	Accession	% Identity
Clade I			
264/182	S1-s-6-15-13473-K4 - Mangrove sediments; Mai Po Marshes	GQ331373.1	89-90
240/174	C11-14717-I3 hzo - Mangrove sediments; Mai Po Marshes	HM209720.1	89-91
293	C3-hzo-70 - Surface sediment; Pearl Estuary	KF935104.1	89
298	S1-s-6-15-13473-K4 - Mangrove sediments; Mai Po Marshes	GQ331373.1	91
43/8/176	77 - Freshwater lake sediment; Yangtze River Delta	KF594253.1	89
Clade II			
250/244/190	Rushing_14_HZO – Groundwater; North Carolina	HM851922.1	96-97
17/21	Crosby_9_HZO – Groundwater; North Carolina	HM851937.1	96-97
56	GZNAna6 – Sediment; Dongjiang River	JX069682.1	98
Clade III			

109	Crosby_10_HZO – Groundwater; North Carolina	HM851938.1	94
254	Rushing_14_HZO – Groundwater; North Carolina	HM851922.1	94
97/26/166/260/214/267	Rushing_14_HZO – Groundwater; North Carolina	HM851922.1	94-96
108/186/233/282	QTWAna25 – Water column; Dongjiang River	JX069733.1	93-95
13	Crosby_6_HZO – Groundwater; North Carolina	HM851934.1	96
281	Neal_16_HZO – Groundwater; North Carolina	HM851904.1	94
142/228/170/307	Rushing_16_HZO – Groundwater; North Carolina	HM851924.1	96-97
Clade IV			
5/96/203/12/311/9/121	Shzo62 - Wetland soil; Seine Estuary	KM250446.1	96-97
Others			
272	117 - Freshwater lake sediment; Yangtze River Delta	KF594282.1	97
256	125 - Freshwater lake sediment; Yangtze River Delta	KF594287.1	96
195	128 - Freshwater lake sediment; Yangtze River Delta	KF594289.1	96
147/102	170 - Freshwater lake sediment; Yangtze River Delta	KF594317.1	96-97
258	175 - Freshwater lake sediment; Yangtze River Delta	KF594319.1	97
4/279/165	192 - Freshwater lake sediment; Yangtze River Delta	KF594329.1	96-97
216	195 - Freshwater lake sediment; Yangtze River Delta	KF594331.1	96
257	47 - Freshwater lake sediment; Yangtze River Delta	KF594232.1	98
71/0/194	51 - Freshwater lake sediment; Yangtze River Delta	KF594236.1	97-98

6	C2-hzo-25 - Surface sediment; Pearl Estuary	KF935025.1	95
278/79/206/212/196	FH0-18 - Freshwater aquaculture pond; China	KF156975.1	96-98
11/15/69/229/277	P3-hzo-50 - Surface sediment; Pearl Estuary	KF934861.1	96
300/248/268	P7-hzo-17 - Surface sediment; Pearl Estuary	KF934877.1	94-95
224/274	Shzo52 - Wetland soil; Seine Estuary	KM250452.1	97-98
42/106/164/169/204/262/117/ 129/154/181/261/310/3	Shzo53 - Wetland soil; Seine Estuary	KM250443.1	96-98
152/133	Shzo54 - Wetland soil; Seine Estuary	KM250451.1	97-98
44/234	Shzo65 - Wetland soil; Seine Estuary	KM250447.1	98
232	SPhzo13 - Wetland soil; Seine Estuary	KM250427.1	97
312/316/219/290/303	SPhzo15 - Wetland soil; Seine Estuary	KM250429.1	96-97
61/112/318	SPhzo7 - Wetland soil; Seine Estuary	KM250436.1	98
20	Crosby_6_HZO – Groundwater; North	HM851934.1	92

Table S7: Concentration of nitrate/nitrite (NO_χ^-) and ammonium in slurries before the addition of $^{15}NH_4^+$ (reference samples) and $^{15}NO_\chi^-$ during the incubation. Reference concentrations are mean values ± 1 standard error, $^{15}NO_\chi^-$ data are third quartile concentrations with maximum values in parenthesis.

	Concentration (μM)		
Site Label	NH_4^+ (reference)	NO_χ^- (reference)	$^{15}NO_\chi^-$ (time series)*
Clay 1	422 ± 29	1.7 ± 0.7	BDL (BDL)
Clay 2	560 ± 47	0.3 ± 0.1	BDL (BDL)
Clay 3	464 ± 25	0.6 ± 0.2	BDL (BDL)
Sand 1	346 ± 37	3.0 ± 3.0	0.06 (28.3)
Sand 2	354 ± 37	0.3 ± 0.1	0.20 (25.6)
Sand 3	559 ± 127	0.7 ± 0.1	1.1 (29.2)
Chalk 1	958 ± 96	0.7 ± 0.3	0.03 (8.0)
Chalk 2	796 ± 48	0.8 ± 0.2	BDL (3.2)
Chalk 3	676 ± 52	0.7 ± 0.1	BDL (1.1)

*BDL denotes below detection limit (0.02 μmol $^{15}NO_\chi^-$ L^{-1}).

Table S8: ^{15}N-labelling of NH_4^+, NO_χ^- and N_2 pools measured during oxic incubations with $^{15}NH_4^+$ and predicted ^{15}N labelling of N_2 resulting from denitrification or anammox. Each time series experiment consisted of 5 measurements, data represent the median proportion of ^{15}N, where a proportion of 1 = 100% ^{15}N.

	Measured			Modelled		
Site Label	NH_4^+	NO_χ^-	N_2	Denitrification -N_2	Anammox-N_2	ΔN_2*
Time series experiments with $^{15}NO_\chi^-$ that met model criteria†						
Sand 1	0.69	0.41	0.50	0.41	0.51	
	0.74	0.42	0.53	0.42	0.54	
	0.78	0.59	0.67	0.59	0.67	
Sand 2	0.67	0.50	0.53	0.50	0.57	
	0.76	0.32	0.37	0.32	0.40	
Sand 3	0.63	0.41	0.41	0.41	0.50	
Chalk 1	0.50	0.37	0.39	0.37	0.42	
Chalk 2	0.59	0.34	0.38	0.34	0.43	
Time series experiments with $^{15}NO_\chi^-$ that did not meet model criteria						
Sand 1	0.58	0.26	0.47	0.26	0.36	0.11
Sand 3	0.63	0.20	0.59	0.20	0.29	0.30
	0.63	0.36	0.66	0.36	0.46	0.20
Chalk 1	0.50	0.42	0.59	0.42	0.45	0.14
Chalk 2	0.67	0.01	0.14	0.01	0.01	0.13
Chalk 3	0.59	0.01	0.66	0.01	0.01	0.65

*ΔN_2 is the deviation in the measured ^{15}N-N_2 pool from the maximum model prediction. The ^{15}N-labelling of N_2 in the time series experiments that met model criteria were within the bounds of the model and ΔN_2 is, therefore, not applicable. †For a successful model $^{15}NO_\chi^-$ must be present in the slurry and the ^{15}N-labelling of the produced N_2 must fall between the anammox and denitrification endmembers. *See* "Contribution of anammox and denitrification to N_2 production in oxic slurries" below for more information.

Table S9: Ambient denitrification activity across rivers of contrasting geology. Rates were determined via direct, in situ measurements. Data are means ± 1 standard error.

	Denitrification Rate (μmol N m^{-2} h^{-1})	
Site Label	Site	Geology
Clay 1	269 ± 50	243 ± 229
Clay 2	218 ± 26	
Sand 1	34 ± 3	28 ± 4
Sand 2	22 ± 3	
Chalk 1	26 ± 1	38 ± 3
Chalk 2	49 ± 3	

Supplementary Figures

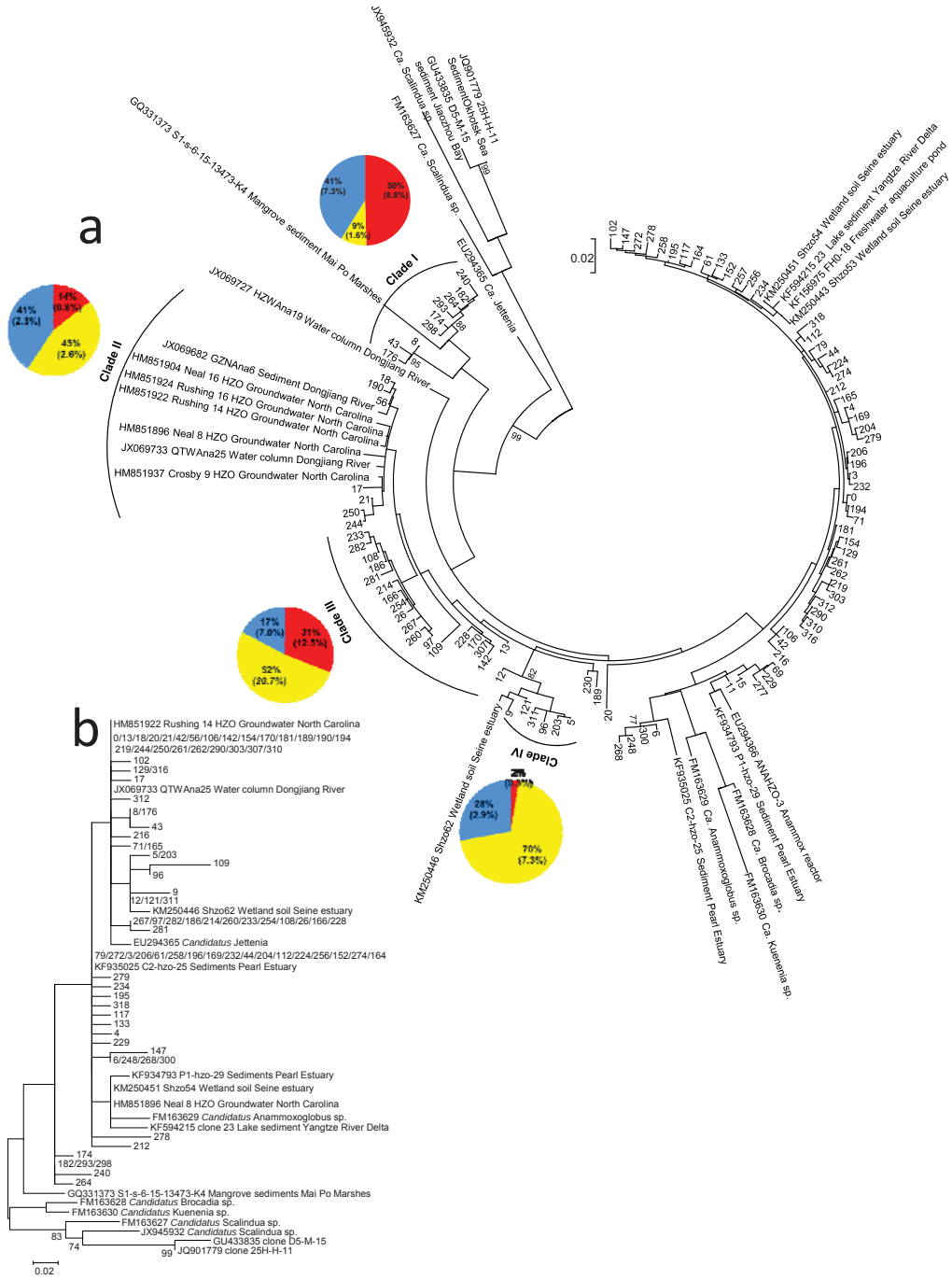

Figure S1: Phylogeny of *hzo* nucleotide gene sequences (a), and unique amino acid sequences (b). Trees were constructed using Maximum Likelihood methods from the 100 most abundant OTUs, which represent 92-93% of all sequences recovered (see Methods). Branch lengths reflect the number of substitutions per site. Bootstrap values >70% are shown. Pie charts show relative distribution across chalk (yellow), sand (blue) and clay (red) sediments of sequences assigned to OTUs within each clade. Percentages in brackets show the total percentage of sequences assigned to OTUs within each clade for each geology. Representative closest relatives by DNA sequence identity (BLASTn) are shown.

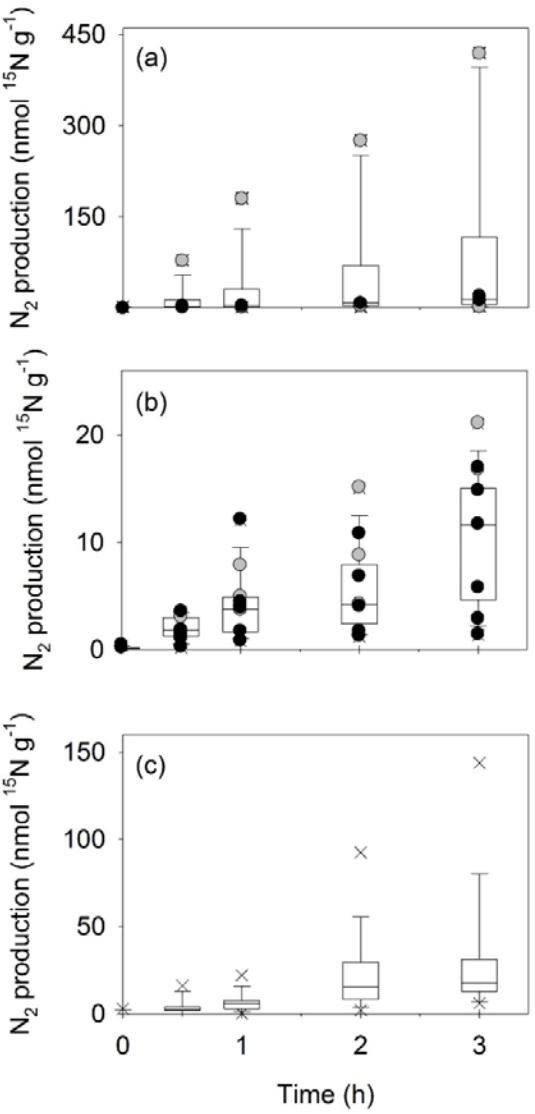

Figure S2: **Production of ^{15}N-N_2 following addition of $^{15}NH_4^+$ to oxic slurries of chalk-gravels (a), sands (b), and clays (c).** Box plots summarise all data with the interquartile range, minimum and maximum, median and outliers represented by the box, whiskers, horizontal line and crosses, respectively. Data from incubations containing measurable $^{15}NO_\chi^-$ overlay the box plots. Black circles are incubations where ^{15}N-labelling of produced N_2 was within the predicted anammox and denitrification endmembers (n=2 and 6 for chalk and sand, respectively). Grey circles represent incubations where produced N_2 was ^{15}N-enriched relative to the endmembers (n=3 for both chalk and sand).

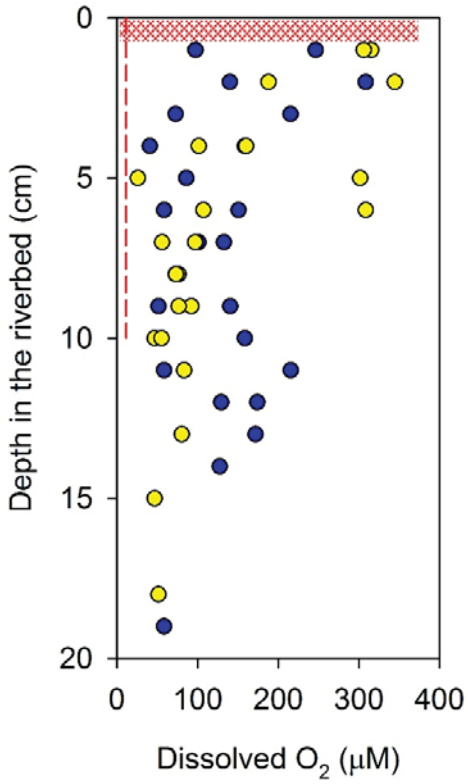

Figure S3: Porewater oxygen varies in sediments of differing permeability. Circles are measurements performed on porewater recovered from sands (blue) or chalk-gravels (yellow) with a depth resolution of approximately 1cm using mini-probes. The dashed line is the average oxygen concentration of clay porewater recovered via rhizon samplers with a 10cm screened interval. The shaded area is the depth of O_2 penetration in clays determined with a micro-profiler.

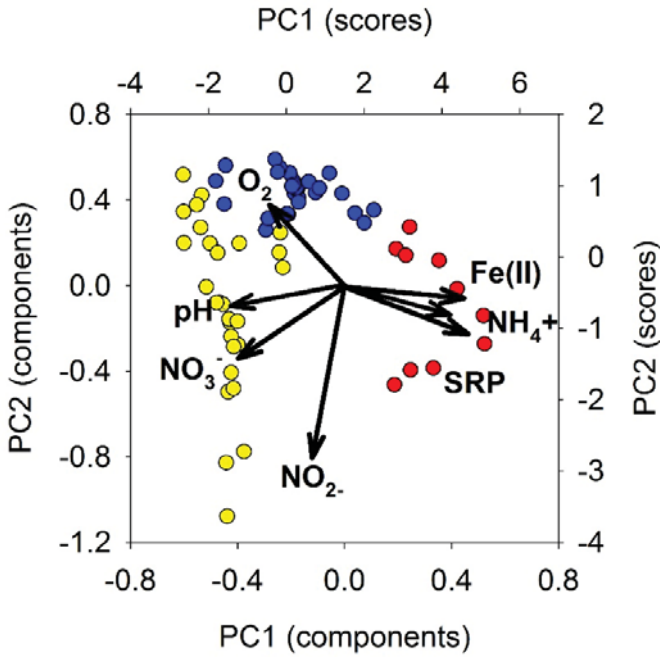

Figure S4: Gradients of porewater chemistry within riverbeds of different permeability as determined through principal components analysis. Data are shown in a correlation bi-plot and were scaled and centred during the analysis. Principal components 1 and 2 accounted for 56% and 19% of the variance, respectively. Arrows are vectors representing chemical variables (SRP and Fe(II) denote soluble reactive phosphorus and iron (II), respectively) and circles are scores from individual samples from clay (red), sand (blue) and chalk-gravel dominated riverbeds.

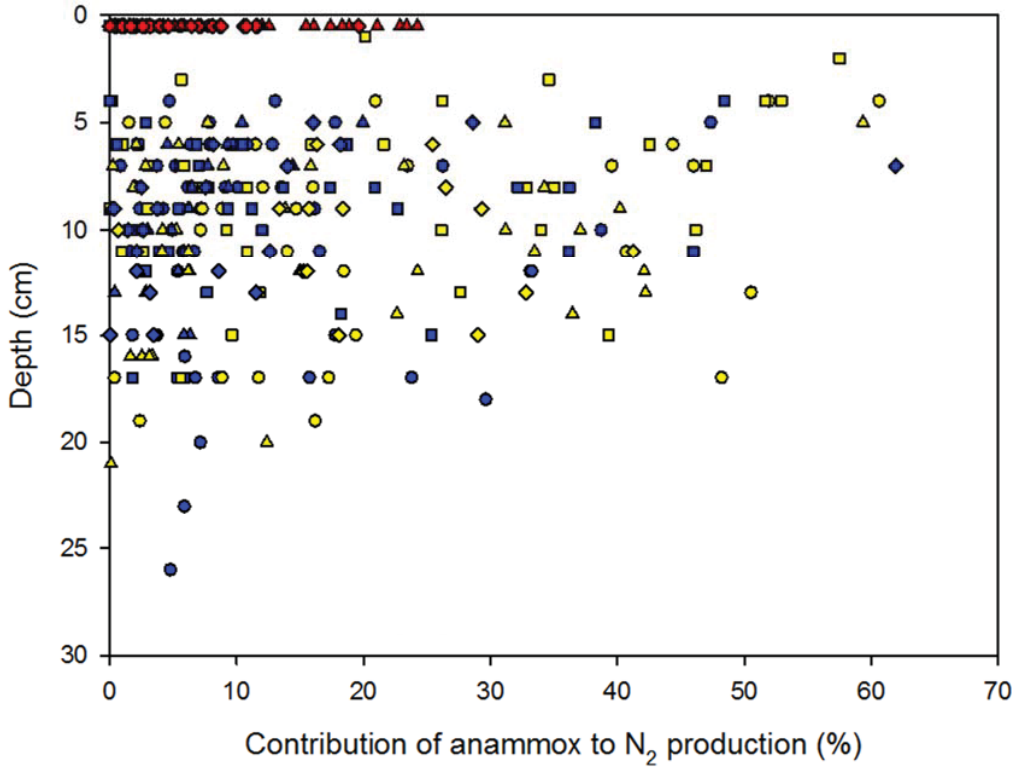

Figure S5: Temporal distribution of anammox activity in riverine sediments. Data are from spring, summer, autumn and winter field campaigns (circles, squares, triangles and diamonds, respectively). The summer data shown here are the focus of the manuscript however overall patterns in the contribution of anammox to N_2 production are consistent throughout the seasons; chalk (yellow) > sand (blue) > clay (red). There is no data from one river (sand) in autumn and two rivers (sand, chalk) in winter as flooding prevented safe access to the sites.

Supplementary discussion 1: Analysis of *hzo* gene seqeunces

The anammox functional *hzo* gene was sequenced (>1.57 million sequences clustered into 316 OTUs, 95 % similarity), with an average of 58,000 reads per sample. Phylogenetic analysis of *hzo*) revealed four clades (Clade I-IV) (Figure S1a) that differed in their relative distributions between the three geologies. In general, our *hzo* sequences were distinct from known *hzo* sequences (BLASTn; Table S6). For example, Clade I had only 89-91 % sequence identity to uncultured anammox bacterium clones from mangrove and estuary sediments, whilst OTUs 8, 43, and 176, were more related to *hzo* sequences from an uncultured anammox bacterium clone from the Yangtze River Delta (Table S6). OTUs in Clade II were less dominant in clays, sharing 94-97 % identity with clones from groundwater and for Clade III, 52 % were recovered from chalk rivers that comprised 21 % of total chalk sequences (Figure S1). OTUs 108, 186, 233 and 282, in Clade III, had 93-95 % sequence identity to an uncultured anammox bacterium clone (Table S6) from the Dongjiang River.[2] Some 70% of Clade IV sequences were from chalk rivers, comprising 7.3 % of total chalk sequences, which shared 96-97 % identity to a riparian soil anammox clone (Seine Estuary)[3] (Table S6). Our river sediments show a broad diversity of *hzo* sequences which are distinct from known low-diversity *hzo* sequences from marine sediments (Figure S1).

The 100 unique *hzo* nucleotide OTU sequences yielded 32 unique amino acid sequences (Figure S1) with both sets of sequences being more closely related to *hzo* sequences from *Ca*. Anammoxoglobus, *Ca*. Brocadia and *Ca*. Jettenia, rather than marine *Ca*. Scalindua species (Figure S1).

Supplementary methodology

Description of sites

Nine rivers in the Hampshire Avon catchment were the focus of this study (Table S1). Much of the Hampshire Avon catchment consists of permeable chalk from the Upper Chalk formation underlain by less permeable Upper Greensand and impermeable Gault clay formations.[4] Sizeable outcrops of Greensand occur in the north and west of the catchment whilst outcrops of clay are restricted to a single region[5] (areal extent ≈ 13 and 1 % of total catchment area for greensand and clay). We selected three rivers within sub-catchments of predominantly one geology to investigate anammox activity across a gradient of riverbed permeability. In the Upper Chalk these were the R. Ebble, R. Wylye and R. Avon (east branch) at Rushall. In the Greensand the rivers sampled were the Nadder and Avon (west branch) at Marden and Rushall and, in the clay (impermeable), the R. Sem and two of its tributaries were included. Some of the rivers were 1st order streams (e.g. the tributaries of the Sem) whilst others were 2nd or 3rd order. At the time of sampling river widths were <5 m and depths <1 m, on average, and discharge was primarily base flow. Land use within the river sub-catchments is predominantly agricultural (arable grassland, dairy farming) but includes some small villages (<7.5 % total catchment area)[4] and patches of forest.

Measurement of anammox activity - synthetic river water

We were not able to use river water from our study sites to prepare slurries as standard methods for determination of anammox and denitrification potential require all ambient $^{14}NO_{\chi}^{-}$ to be removed prior to the experiment.[6,7] In the Hampshire Avon catchment ambient nitrate concentrations are very high: e.g. 100-200 μM in clay-based rivers and 300-500 μM in permeable rivers (unpublished data). The length of pre-incubation required to remove such large amounts of $^{14}NO_3^-$ from the slurry would likely alter the microbial community and

availability of substrates (e.g. labile carbon). Instead we use synthetic river water as per the media in Smart and Barko[8] as slurry water and tracer matrix in potential and *in situ* measurements, respectively. For both types of experiments we add carbonate to the media (~2 mM and ~5 mM final dissolved inorganic carbon concentration for clays and sands, and chalks, respectively), adjusting the pH back to ~7 with dilute HCl (if necessary) to better represent the rivers studied. For *in situ* measurements, KCl is also added (final concentration 4 mM) for use as a conservative tracer.

Calculations for activity measurements

Converting raw mass spectrometer signals to concentrations. Individual mass spectrometer signals from N_2 analysis (i.e. mass-to-charge ratio = 28, 29 or 30) were adjusted for drift assuming linear changes between standards at the beginning and end of a batch of samples, typically 10. Drift control standards consisted of the same matrix as samples, i.e. oxygen free nitrogen for anoxic slurries, air for oxic slurries or helium over air equilibrated water for core or porewater samples, and were analysed at least every 10 samples. Corrected mass spectrometer signals were converted to excess aqueous $^{29}N_2$ or $^{30}N_2$ concentrations (combinations of ^{14}N-^{15}N and ^{15}N-^{15}N, respectively) after correction for drift as follows:[9]

$$^{x}N_2\ (\mu\text{moles L}^{-1}) = \left[\left(\frac{^{m}N_2}{\sum N_2}\right)_{sample} - \left(\frac{^{m}N_2}{\sum N_2}\right)_{reference}\right] \text{ x } \sum N_2 \text{ x } \alpha \text{ x } V_s^{-1} \qquad (1)$$

Where x can be $^{29}N_2$ or $^{30}N_2$; $^{m}N_2$ is the area from mass-to-charge ratio 29 or 30; ΣN_2 is the sum of all areas (i.e. mass-to-charge ratio 28 + 29 + 30); α is the calibration factor (μmoles N_2 vial^{-1}: ΣN_2 for initial drift control standard) and V_s is the volume of water in the vial (L vial^{-1}). 'Sample' refers to a treatment with ^{15}N added whilst 'reference' denotes a sample to which no ^{15}N was added, or in the case of *in situ* measurements, a sample taken prior to the

$^{15}NO_3^-$ injection. For slurries, excess aqueous concentrations were converted further to the total amount of $^{29}N_2$ or $^{30}N_2$ produced per gram of dry sediment:

$$^{x}N_2\ (\mu mol\ g^{-1}) = \left(V_{aq}\ x\ \left[{}^{x}N_2 \right]_{aq} + V_{h/sp}\ x\ \left[{}^{x}N_2 \right]_{h/sp} \right) x\ M_s^{-1} \quad (2)$$

where V_{aq} and $V_{h/sp}$ are the volume (L) of the aqueous phase and headspace of the slurry, respectively; $[^xN_2]_{aq}$ is the aqueous concentration of $^{29}N_2$ or $^{30}N_2$ from equation 1; $[^xN_2]_{h/sp}$ is the concentration of $^{29}N_2$ or $^{30}N_2$ in the headspace and was calculated using the Bunsen solubility coefficient[10] for N_2 and the aqueous concentration from equation 1. M_s is the dry weight of sediment in the slurry (g). To express production of ^{15}N-labelled N_2 in terms of N the following equation was used:[11]

$$\text{Production of } ^{15}N\text{-}N_2\ (\mu moles\ L^{-1} \text{ or } \mu moles\ g^{-1}) = P_{29} + 2\ x\ P_{30} \quad (3)$$

where P_{29} and P_{30} are the production of $^{29}N_2$ or $^{30}N_2$ from equations 1 or 2. Values expressed as μmol L^{-1} or μmol g^{-1} were converted to rates by (i) dividing the value by the incubation time when samples consisted of a T_{final} and a reference sample or (ii) plotting data as a function of incubation time, applying a trendline to the linear portion of the time series and entering the resultant slopes (b_1) into equation 3.

Anammox and denitrification potential in anoxic slurries. Total anammox and denitrification potential (A_{total} and D_{total}, respectively) and the contribution of anammox to N_2 production in slurries amended with $^{15}NO_3^-$ was calculated as follows:[12]

$$A_{total}\ (nmol\ N_2\ g^{-1}\ h^{-1}) = F_{NO_3^-}^{-1}\ x\ \left[P_{29} + 2\ x\ (1\text{-}F_{NO_3^-}^{-1})\ x\ P_{30} \right] \quad (4)$$

$$D_{total}\ (nmol\ N_2\ g^{-1}\ h^{-1}) = P_{30}\ x\ F_{NO_3^-}^{-1} \quad (5)$$

$$\text{Contribution of anammox (\%)} = \frac{A_{total}}{A_{total} + D_{total}}\ x\ 100 \quad (6)$$

Where $F_{NO_3^-}$ is the proportion of ^{15}N in the nitrate pool of the slurry (= 0.98, i.e., the same as ^{15}N-labelling of the tracer as all $^{14}NO_\chi^-$ was removed in the pre-incubation). Anammox

potentials plotted in Figure 1a were calculated via equation 4 and multiplied by 2 to convert nmol N_2 to nmol N.

Contribution of anammox and denitrification to N_2 production in oxic slurries. We initially intended for our oxic incubations with $^{15}NH_4^+$ to be a nitrification assay, where the rate of $^{15}NO_\chi^-$ production would be representative of net nitrification. We analysed the headspace of the oxic slurries for ^{15}N-N_2 expecting to find no $^{29}N_2$ or $^{30}N_2$ as per our previous studies in less reactive sediments (unpublished data, but *see* study reported in ref. 13). To our surprise, however, we measured clear production of $^{29}N_2$ and some minor production of $^{30}N_2$ in all samples. To estimate anammox and denitrification potential using equations 4 and 5, denitrification must be the only pathway that can produce $^{30}N_2$ (ref. 12). In our oxic slurries we deliberately added $^{15}NH_4^+$ and, therefore, this assumption cannot be met as anammox could also produce $^{30}N_2$ (oxidation of $^{15}NH_4^+$ and reduction of nitrification-derived $^{15}NO_\chi^-$). To apportion N_2 production to anammox or denitrification we compared the ^{15}N-labelling of the produced N_2 to the ^{15}N-labelling of N_2 predicted to be produced solely by anammox or denitrification in a mixing model, as follows:

$$^{15}\text{N labelling of produced N}_2\ (F_{P_{N_2}}) = \frac{1}{1 + \left(\frac{P_{29}}{2 \text{ x } P_{30}}\right)} \quad (7)$$

$$\text{Anammox endmember } (F_{N_2\ anammox}) = \frac{1}{1 + \left(\frac{\left[\left(1 - F_{NH_4^+}\right) \text{ x } F_{NO_\chi^-}\right] + \left[\left(1 - F_{NO_\chi^-}\right) \text{ x } F_{NH_4^+}\right]}{2 \text{ x } F_{NH_4^+} \text{ x } F_{NO_\chi^-}}\right)} \quad (8)$$

$$\text{Denitrification endmember } (F_{N_2\ denitrification}) = F_{NO_\chi^-} \quad (9)$$

$$\text{Contribution of anammox (proportion)} = 1 - \frac{F_{P_{N_2}} - F_{N_2\ anammox}}{F_{N_2\ denitrification} - F_{N_2\ anammox}} \quad (10)$$

where $F_{NO_\chi^-}$ is the proportion of ^{15}N in the NO_χ^- pool as determined by the sulphamic acid assay and $F_{NH_4^+}$ is the proportion of ^{15}N in the NH_4^+ pool, estimated by the increase in the ammonium concentration of the slurry following addition of the tracer.[11,14,15] The assumption that ^{15}N-labelling of N_2 produced solely through denitrification is equal to that of the NO_χ^- pool (i.e. equation 9) is fundamental to the isotope pairing technique.[11,16] The distribution of isotopes within N_2 produced via anammox assumes random pairing of one NH_4^+-N and one NO_χ^--N where the probability of $^{28}N_2$, $^{29}N_2$ or $^{30}N_2$ formation and can be predicted as follows:[17]

$$\text{Probability of } {}^{28}N_2 = (1 - F_{NH_4^+}) \text{ x } (1 - F_{NO_\chi^-})$$

(11) $$\text{Probability of } {}^{29}N_2 = \left(F_{NH_4^+} \text{ x } (1-F_{NO_\chi^-})\right) + \left(F_{NO_\chi^-} \text{ x } (1-F_{NH_4^+})\right)$$

(12) $$\text{Probability of } {}^{30}N_2 = F_{NH_4^+} \text{ x } F_{NO_\chi^-}$$

(13)

Use of equations 9 to 13 to apportion N_2 production to anammox or denitrification requires the ^{15}N-labelling of the NH_4^+, NO_χ^- and N_2 pools to be known. In our experiment, background concentrations of NO_χ^- were low (Table S7) and nitrification supplied NO_χ^- to the sediments. If coupling between nitrification and N_2 production is tight, NO_χ^- may not accumulate in the bulk porewater, as was the case for the majority of our slurries (31 out of 45). Here, as nitrification likely creates all NO_χ^-, $F_{NO_\chi^-}$ and $F_{NH_4^+}$ must be equal and the contribution of anammox and denitrification to N_2 production cannot be determined.[17] Similarly, to apportion N_2 production to either anammox or denitrification using the above equations the labelling of the produced N_2 must fall between the two endmembers. In our experiment, 6 slurries that contained measurable NO_χ^- failed this criteria as the produced N_2 was more enriched in ^{15}N than either of the endmembers. Heterogeneity in the ^{15}N content of

reactants and products has previously been attributed to internal shunting of nitrite between reaction pathways without mixing with the bulk nitrite pool.[18]

Estimating *in situ* anammox and denitrification activity. Rates of ambient N_2 production were quantified with the revised-isotope pairing technique[16] which uses the rate of ^{15}N-N_2 production and $F_{NO_\chi^-}$ (but expressed as r_{14}, *see* below) to estimate genuine $^{28}N_2$ production from ambient $^{14}NO_x^-$:

$$\text{Rate of ambient } N_2 \text{ production } (\mu\text{mol N L}^{-1}\ \text{h}^{-1}) = 2 \text{ x } r_{14} \text{ x } \left(P_{29} + P_{30}(1\text{-}r_{14})\right) \quad (14)$$

where r_{14} is the ratio of ^{14}N to ^{15}N within the available nitrate pool. We used the ratio of ^{14}N to ^{15}N in N_2O produced following the addition of $^{15}NO_3^-$ as a proxy for r_{14} as N_2O is an intermediate of denitrification, but not anammox, and therefore r_{14}-N_2O reflects the ^{15}N-labelling of the NO_χ^- pool being reduced :[19]

$$r_{14}\text{-}N_2O = \frac{\left(\frac{^{45}N_2O}{\sum N_2O}\right)_{\text{sample}} - \left(\frac{^{45}N_2O}{\sum N_2O}\right)_{\text{reference}}}{2 \text{ x } \left(\left(\frac{^{46}N_2O}{\sum N_2O}\right)_{\text{sample}} - \left(\frac{^{46}N_2O}{\sum N_2O}\right)_{\text{reference}}\right)} \quad (15)$$

where $^{45}N_2O$ and $^{46}N_2O$ are areas for mass-to-charge ratio 45 and 46, respectively and ΣN_2O is the sum of all areas (i.e. mass-to-charge ratio 44 + 45+ 46). To determine the contribution of anammox to N_2 production, calculated via equation 14, we compared the ^{15}N-labelling of the N_2O and N_2 produced following addition of $^{15}NO_3^-$ as follows:[19]

$$F_{P_{N_2O}} = \frac{1}{1 + r_{14}\text{-}N_2O} \quad (16)$$

$$\text{Contribution of anammox (\%)} = \frac{2 - 2 \text{ x } \frac{F_{P_{N_2}}}{F_{P_{N_2O}}}}{2 - \frac{F_{P_{N_2}}}{F_{P_{N_2O}}}} \text{ x } 100 \quad (17)$$

with $F_{P_{N_2}}$ as per equation 7. Ambient rates of anammox were calculated by multiplying the ambient rate of N_2 production by the contribution of anammox (as a proportion; equations 14 and 17, respectively). Ambient rates of denitrification were the difference between total ambient N_2 production (equation 14) and ambient anammox. For sediment core data, volumetric rates were converted to areal rates (i.e. from μmol N L^{-1} homogenised core h^{-1} to μmol N m^{-2} riverbed h^{-1}) by scaling up with the dimensions of the core (e.g. sediment porosity, volume of overlying water and surface area of sediment). For permeable sediments, areal rates were obtained by integrating depth profiles (~4 to ~ 20cm) of volumetric anammox or denitrification rates (μmol N L^{-1} porewater h^{-1}) using the trapezium rule.

Calculation of base-flow index. The baseflow index (BFI) is normally computed using techniques to separate the stream discharge hydrographs into slow and fast flow components. For the study here we estimated BFI (Table S2) from a rainfall runoff model computed hydrograph utilising the catchment topography and soil type based on the Hydrology Of Soil Types (HOST) classification.[20]

References

1 Lansdown, K. *et al.* Fine-Scale in Situ Measurement of Riverbed Nitrate Production and Consumption in an Armored Permeable Riverbed. *Environ. Sci. Technol.* **48**, 4425-4434 (2014).

2 Sun, W. *et al.* Diversity and distribution of planktonic anaerobic ammonium-oxidizing bacteria in the Dongjiang River, China. *Microbiol. Res.* **169**, 897-906 (2014).

3 Naeher, S. *et al.* Molecular and geochemical constraints on anaerobic ammonium oxidation (anammox) in a riparian zone of the Seine Estuary (France). *Biogeochemistry* **123**, 237-250 (2015).

4 Jarvie, H. P. *et al.* Role of river bed sediments as sources and sinks of phosphorus across two major eutrophic UK river basins: the Hampshire Avon and Herefordshire Wye. *J. Hydrol.* **304**, 51-74 (2005).

5 Jarvie, H. P., Neal, C., Withers, P. J. A., Wescott, C. & Acornley, R. M. Nutrient hydrochemistry for a groundwater-dominated catchment: The Hampshire Avon, UK. *Sci. Total Environ.* **344**, 143-158 (2005).

6 Trimmer, M., Nicholls, J. C. & Deflandre, R. Anaerobic ammonium oxidation measured in sediments along the Thames Estuary, United Kingdom. *Appl. Environ. Microbiol.* **69**, 6447 - 6454 (2003).

7 Risgaard-Petersen, N. *et al.* Anaerobic ammonium oxidation in an estuarine sediment. *Aquat. Microb. Ecol.* **36**, 293 - 304 (2004).

8 Smart, R. M. & Barko, J. W. Laboratory culture of submersed freshwater macrophytes on natural sediments. *Aquat. Bot.* **21**, 251 - 263 (1985).

9 Thamdrup, B. & Dalsgaard, T. The fate of ammonium in anoxic manganese oxide-rich marine sediment. *Geochim. Cosmochim. Acta* **64**, 4157 - 4164 (2000).

10 Weiss, R. F. The solubility of nitrogen, oxygen and argon in water and seawater. *Deep-Sea Res.: Oceanogr. Abstr.* **17**, 721-735 (1970).

11 Nielsen, L. P. Denitrification in sediment determined from nitrogen isotope pairing. *FEMS Microbiol. Ecol.* **86**, 357 - 362 (1992).

12 Thamdrup, B. & Dalsgaard, T. Production of N_2 through anaerobic ammonium oxidation coupled to nitrate reduction in marine sediments. *Appl. Environ. Microbiol.* **68**, 1312 - 1318 (2002).

13 Lansdown, K. *et al.* Characterization of the key pathways of dissimilatory nitrate reduction and their response to complex organic substrates in hyporheic sediments. *Limnol. Oceanogr.* **57**, 387 - 400 (2012).

14 Jensen, M. M. *et al.* Intensive nitrogen loss over the Omani Shelf due to anammox coupled with dissimilatory nitrite reduction to ammonium. *ISME J.* **5**, 1660-1670 (2011).

15 Nicholls, J. C. & Trimmer, M. Widespread occurrence of the anammox reaction in estuarine sediments. *Aquat. Microb. Ecol.* **55**, 105 - 113 (2009).

16 Risgaard-Petersen, N., Nielsen, L. P., Rysgaard, S., Dalsgaard, T. & Meyer, R. L. Application of the isotope pairing technique in sediments where anammox and denitrification coexist. *Limnol. Oceanogr. Methods* **1**, 63 - 73 (2003).

17 Spott, O. & Stange, C. F. A new mathematical approach for calculating the contribution of anammox, denitrification and atmosphere to an N_2 mixture based on a ^{15}N tracer technique. *Rapid Commun. Mass Sp.* **21**, 2398-2406 (2007).

18 de Brabandere, L. *et al.* Vertical partitioning of nitrogen-loss processes across the oxic-anoxic interface of an oceanic oxygen minimum zone. *Environ. Microbiol.* **16**, 3041-3054 (2014).

19 Trimmer, M., Risgaard-Petersen, N., Nicholls, J. C. & Engström, P. Direct measurement of anaerobic ammonium oxidation (anammox) and denitrification in intact sediment cores. *MEPS* **326**, 37-47 (2006).

20 Boorman, D. B., Hollis, J. M. & Lilly, A. *Hydrology of Soil Types: a hydrologically-based classification of the soils of the United Kingdom*. (Insitute of Hydrology, 1995).